Journal of the Iranian Chemical Society (2023) 20:1629–1642
https://doi.org/10.1007/s13738-023-02783-0

ORIGINAL PAPER

Enhancement of CO_2 absorption and heat transfer properties using amine functionalized magnetic graphene oxide/MDEA nanofluid

Anahita Lashgarinejad[1] · Seyedeh Shadi Hosseini[1] · Vahid Irani[1] · Mohammad H. Ghasemi[1] · Raha Mohammadpour[1] · Ahmad Tavasoli[1]

Received: 9 December 2022 / Accepted: 11 March 2023 / Published online: 29 March 2023

Abstract
Amino-functionalized magnetic graphene oxide is added to MDEA solution to improve the CO_2 absorption. Graphene oxide (GO) was synthesized and functionalized by amine groups and magnetic materials (NH_2-mGO). NH_2-mGO was fully characterized using XRD, FTIR, SEM, EDS, TEM, and BET techniques. The presence of O, Fe, and N elements with weight percentages of 21.51, 9.43, and 5.61 indicated that graphene surfaces were well functionalized with ethylenediamine and magnetic Fe_3O_4 nanoparticles. 0.1 wt.% NH_2-mGO was added to the 40 wt.% aqueous MDEA solution to obtain a novel absorption solution known as nanofluid. CO_2 absorption experiments were conducted at different temperatures and pressures and the results showed that the absorption has been improved by 19% compared with the base fluid (40 wt.% aqueous MDEA solution). Thermal conductivity of the nanofluid was examined and results revealed an increase of about 17% in the thermal conductivity of the nanofluid compared to the base fluid. Convective heat transfer investigations also showed an average improvement of 15% after the addition of nanoparticles into the fluid. NH_2-mGO had the ability to effectively recovered and retain its active sites on the surface throughout the repeated cycles and thermal treatment. The magnetic property of the as-prepared nanostructure allowed recovering the spent nanoparticles for using in the subsequent absorption process.

Keywords CO_2 absorption · NH_2-mGO · Nanofluid · Thermal conductivity · Convective heat transfer

Introduction

Carbon dioxide (CO_2) emissions resulted from human activities need urgent action to prevent global warming and climate change [1–8]. Development of carbon capture and storage (CCS) technology is one of the key solutions to overcome some limitations associated with environmental problems [4, 9–11]. There are different technologies including amine solvents [12], membranes [13, 14], adsorption by solid-based sorbents [15, 16] and cryogenic distillation [17]. Among them, amine solvents and solid sorbents have received wide attention due to the high performance and fewer limitations compared with membranes and cryogenic distillation [18].

Amine based solvents, as the most important method in large-scale industrial applications, rely on various amine solvents such as methydiehanolamine (MDEA), monoethanolamine (MEA), diethanolamine (DEA), and triethanolamine (TEA) [19, 20]. MDEA, due to the advantages in the structure (such as stable structure, carbamate formation, and corrosion), is well known as the most popular amine solvent used in the processes leading to high-performance CO_2 absorption [21]. However, CO_2 absorption by amine solvents are costly and corrosive to the equipment as well as require a high energy level [22]. To avoid these disadvantages, more studies and technologies are necessary, such as adsorption by solid sorbent after some modifications in the structure [23].

Various adsorbents have been studied for carbon capture such as zeolites [24], activated carbon [25], metal–organic frameworks (MOFs) [26], aerogels, and graphene oxide [27]. CO_2 capture by these materials is implemented via physisorption and chemisorption processes at a wide range of temperatures and pressures. Numerous studies have focused on actions to improve the selectivity and gas adsorption capacity through some modifications, including amine functionalization and impregnation [21, 24]. However, many solid-based sorbents

✉ Ahmad Tavasoli
tavasoli.a@ut.ac.ir

[1] School of Chemistry, College of Science, University of Tehran, Tehran, Iran

faced problems like blocking off the sorbent pores and poor stability. Therefore, carbon-based sorbents have attracted wide attention because of good thermal/mechanical stability, high surface area and porosity, lower levels of energy for regeneration, and capability to be modified [20]. As functional groups on the surface of the carbon-based materials play an important role in improving the gas capture, many researchers have developed different methods to functionalize these materials to enhance the adsorption capacity [18, 28]. However, solid sorbents are limited due to the availability and low capacity of CO_2 adsorption. Therefore, the combination of amine solutions and nanoparticle adsorbents can be an effective procedure to enhance the absorption rate and minimize the energy required for CO_2 capturing processes [29]. Nanofluids could be a suitable candidate for a combination of these methods because of different advantages including enhancing mass transfer and heat transfer coefficients [30].

A nanofluid system is prepared by the addition of nanoparticles into the base fluid for different applications. Mass transfer and heat transfer are critical factors affecting the gas absorption by amine solvents, and these factors are improved in nanofluids [31]. The addition of low content of nanoparticles into a based-fluid can significantly improve some properties such as mass and heat transfer. The collision of nanoparticles with bubbles available in the fluid leads to smaller bubbles and subsequently enhanced mass transfer [32–36]. The chemical stability of nanofluid should be greatly considered by the ultrasonication of dispersed nanoparticles in the base fluid.

There are various studies focused on CO_2 absorption enhancement using nanofluids. However, the separation of nanoparticles from the nanofluid and regeneration of the solutions containing nanoparticles is known as a problem associated with processes dealing with nanofluids [37–41]. In this study, to solve the above mentioned problem, graphene oxide is modified by Fe_3O_4 and amine functional groups and was added to the 40 wt.% of aqueous MDEA solution. The amine-functionalized magnetic graphene oxide can be separated from the nanofluid by a magnet as well as reused for CO_2 absorption. 0.1 wt.% graphene oxide and amine-functionalized magnetic graphene oxide was separately added to the base fluid and CO_2 absorption experiments were conducted at different temperatures and pressures. It is expected that the magnetic property of the as-prepared nanostructure will allow recovering the spent nanoparticles for using in the subsequent absorption process.

Materials and methods

Materials

All the reagents purchased and used without further purification. CO_2 gas (99.99%) purchased from the Roham gas company (Tehran, Iran). Other reagents used in this study were graphite flakes, sulfuric acid (99.99% H_2SO_4, Sigma-Aldrich), sodium nitrate (70% $NaNO_3$, Sigma-Aldrich), hydrogen peroxide (30% H_2O_2, Merck), potassium permanganate (99.99% $KMnO_4$, Merck), Iron (II) oxide (Fe_3O_4, Merck), ethylene glycol (> 99.0%, Merck) and ammonia water (> 25% NH_4OH, Sigma-Aldrich).

Preparation of graphene oxide (GO)

GO synthesized using modified Hummers method [42]. Briefly, 2 g graphite powder (mesh 500) added to 50 ml concentrated sulfuric acid under stirring condition. Then, 2 g sodium nitrate was added to the solution followed by stirring at 0 °C for 1 h. 7.3 g $KMnO_4$ was slowly added to the mixture and stirred for 2 h. Afterward, mixture temperature was raised to 35 °C and stirred for 2 h. 46 ml distilled water was added along with increasing the temperature to 90 °C and the mixture was stirred for 30 min. Finally, the reaction was stopped by the addition of 140 ml distilled water and 16 ml H_2O_2 (30%) and obtaining a dark brown solution. The as-prepared suspension maintained under ultrasound condition (35 kHz) for 30 min. The obtained GO washed with diluted HCl and distilled water several times until the supernatant fluid became colorless. The dark brown precipitate dried in a vacuum oven at 40 °C for 24 h.

Preparation of magnetic graphene oxide (mGO)

Magnetic graphene oxide (mGO) synthesized using co-precipitation of $FeCl_3$ and $FeCl_2$ on surface of GO nanoparticles [43]. Briefly, GO dispersed in water under vigorous stirring and N_2 atmosphere. Then, $FeCl_3$ and $FeCl_2$ were slowly added to the solution and the obtained mixture was continuously stirred at 85 °C for 1 h. The reduction reaction completed by addition of ammonia water as well as hydrazine hydrate. After cooling the mixture to room temperature, mGO nanoparticles were separated by a magnet, washed with ultra-pure water for several times, and then dried at 60 °C for 20 h.

Preparation of amine-functionalized mGO (NH_2-mGO)

200 mg as-prepared mGO added to 100 ml ethylene glycol solution and the mixture kept under ultrasonic conditions. Then, 1 ml ethylene diamine added to the mixture and the resulted solution transferred to a Teflon autoclave. The solvothermal reaction performed at 200 °C for 7 h. Amine groups bonded covalently through nucleophilic attachment to the oxygen-containing functional groups available on the surface of the GO. The resultant precipitate separated by a magnet and then washed with ultra-pure water several times

to remove the unreacted amine groups. The as-synthesized NH_2-mGO dried at 60 °C for 24 h [22, 44]. The reaction mechanism of the above-mentioned procedures is presented in Fig. 1.

Nanofluid preparation

Nanofluids were prepared via dispersing 0.1wt.% of GO and 0.1wt.% of NH_2-mGO nanoparticles in 40 wt.% aqueous MDEA solutions under ultrasonic agitation at 150 W for 30 min. After preparation of nanofluids, the stability of colloids studied using zeta potential analysis. High zeta potential values (more than ± 25 mV) confirm the stability of nanoparticles in the nanofluids without accumulation [45].

Characterization

The physicochemical properties of as-prepared GO and amine-functionalized magnetic GO were studied using various techniques such as Fourier-transform infrared spectroscopy (FTIR, Bruker-ISS-88), X-ray diffraction (XRD, Xpert MPD diffractometer), transmission electron microscopy (TEM; Jeol JEM-1230, with an acceleration voltage of 100 kV), Brunauer-Emmet-Teller (BET, BELSORP Mini II), scanning electron microscopy (SEM, Tescan), energy dispersive X-ray and thermal gravimetric analysis (TGA, Perkin-Elmer). To investigate the stability of nanofluids, zeta potential analysis performed on a zeta analyzer (Malvern instrument Ltd). XPS analysis was performed on ESCALAB 250 (Thermo Scientific, K-Alpah, USA).

Absorption experiments

Absorption experiments conducted on a double-wall equilibrium cell with a total volume of 290 ml. In this system, the equilibrium cell is connected to a water bath, which is equipped to a pump for circulation of the hot fluid. The fluid circulates in the outside wall and adjusts the temperature of equilibrium cell. The temperature can be measured via a TM-917 Lutron digital thermometer by setting a Pt-100 sensor into the equilibrium cell via a thermowell. The resolution of the thermometer is 0.01 K, which is monitored on a temperature monitor placed in the system. A gas container (with a well-known volume) is connected to the cell and the CO_2 first introduces to this container to obtain the desired pressure at room temperature. Two Baroli type BD sensors (with a pressure range of 0–60 and 0–40 bar and accuracy within 0.1% of full scale) are, respectively, placed on the gas container and equilibrium cell to measure the pressures. The amount of CO_2 introduced to the equilibrium cell is calculated using the methods described at Refs. [46, 47]. The detailed PVT data is obtained from the National Institute of Standards and Technology that provides data for all fluids, including pure CO_2 [18]. So, the total number of moles introduced to the cell is calculated using the following equation:

$$n_{\text{gas}} = \frac{V_C}{RT_a}\left(\frac{P_1}{Z_1} - \frac{P_2}{Z_2}\right) \tag{1}$$

where V_c denotes the volume of the CO_2 container. T_a is the indicative temperature of the CO_2 container (ambient temperature), and R is the universal gas constant, Z_1, Z_2 present the compressibility factors corresponding to the initial and final state in the gas container before and after gas introducing. P_{CO_2} (equilibrium partial pressure of CO_2 in the gas phase of the equilibrium cell) was calculated by:

$$P_{\text{gas}} = P_T - P_V \tag{2}$$

where P_T is the total absolute pressure and P_V is the vapor pressure of solution after reaching a stable state of equilibrium cell, at the low-temperature MDEA has low vapor pressure, so in this work, the vapor phase of MDEA was neglected [48]. The amount of remaining CO_2 in the gas phase was calculated using Eq. (3):

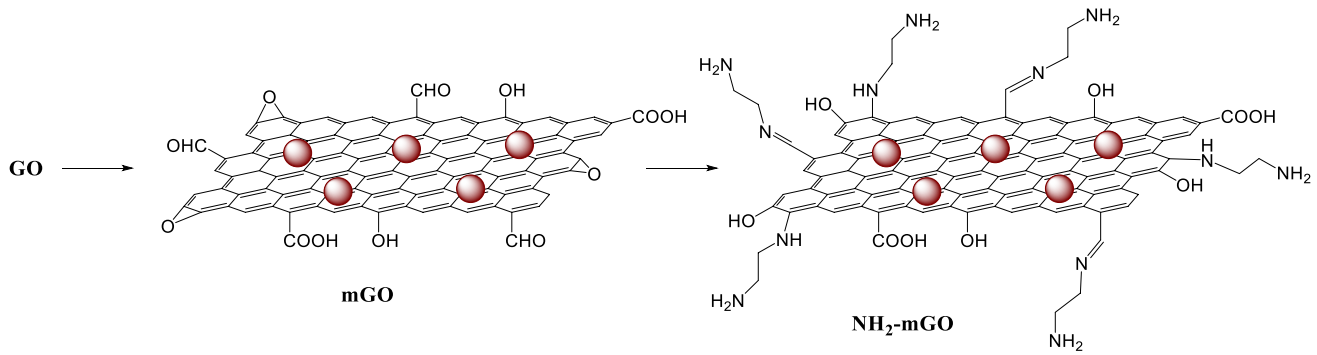

Fig. 1 Schematic reaction mechanism for conversion of GO to mGO and NH2-mGO

$$n_{CO_2}^{g} = \frac{V_g P_{CO_2}}{Z_{CO_2} RT} \tag{3}$$

where V_g is the gas phase volume in the equilibrium cell, Z is the compressibility factor of CO_2 at related P and T, and T is the temperature of the equilibrium cell. The moles of CO_2 in the liquid phase was determined from

$$n_{CO_2}^{l} = n_{CO_2} - n_{CO_2}^{g} \tag{4}$$

And eventually, CO_2 loading in the liquid phase is calculated as

$$m_{CO_2} = \frac{n_{CO_2}^{l}}{w_{sol}} \tag{5}$$

In which w_{sol} is the mass of solvent in kg. The exact volume of the gas phase, V_g, is the difference between the cell volume and the uncharged solvent volume. The errors were determined and then the uncertainties were estimated using the following equation:

$$\delta q = \pm \sqrt{\left[\left(\frac{\partial q}{\partial r}\right)\right]^2 + \ldots + \left[\left(\frac{\partial q}{\partial u}\right).du\right]^2} \tag{6}$$

The volume of the gas container and equilibrium cell were measured by pressure swing experiments (PSE), which is based on the pressure drop occurred between two well-known and unknown volumes, according to the Charles-Gay-Lussac law [49]. The pressure of MDEA in the gas phase was neglected according to the data reported in the literature. The schematic design of the system with all instruments is given in Fig. 2.

The recycling process of the NH_2-mGO

After running the absorption experiments, the NH_2-mGO can be recovered by a magnet. The recycled nanoparticles were then degassed at 150 °C under vacuum overnight before re-running the new experiments. A schematic procedure for recycling the magnetic nanoparticles is presented in Fig. 3.

Thermal conductivity and convective heat transfer measurements

A 60 mm single needle KD2 Pro thermal analyzer (Decagon device, USA) is employed to investigate the thermal conductivity of the nanofluids. Thermal conductivity is examined according to the transient hot-wire method. An abrupt electrical pulse is employed to receive a response (temperature/time) by a probe with a 1.3 mm diameter and 60 mm length. The method was calibrated with deionized water and consequently 20 min remaining the temperature of the probe at a constant value. Three temperatures selected according to the absorption temperature range, including 298, 308, and 318 K, and thermal conductivity measured at these temperatures [50]. A circulator placed in the system to control the temperature and the enhancement rate of the thermal conductivity calculated according to the following equation:

$$\text{Enhancement} = \frac{K_n - K_f}{K_f} \times 100 \tag{7}$$

where K_f and K_n are known as thermal conductivity observed for base fluid and base fluid containing the nanoparticles, respectively.

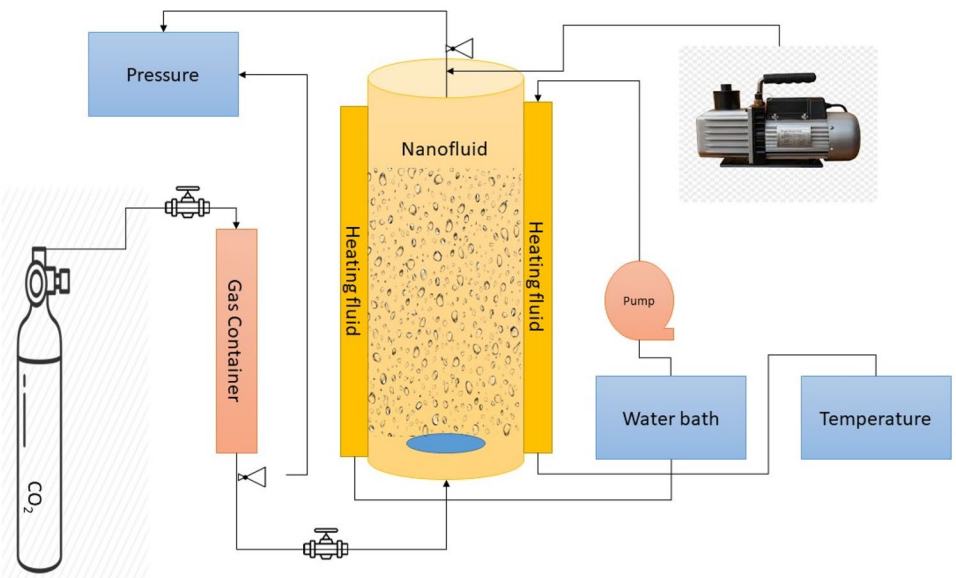

Fig. 2 Schematic design of the system

Fig. 3 Schematic procedure for recycling the magnetic nanoparticles

To study the convective heat transfer coefficient of the nanofluids, a system is used as shown in Fig. 4. The system consists of a test chamber, a reservoir, a pump, and exchanger and a circulator. A copper type tube placed in the test chamber with 11.42 mm diameter and 1 m length. As shown, different places equipped with *K*-type thermocouples to measure the temperature, and finally, the heat transfer coefficient calculated based on the following equation:

$$h(x) = \frac{q^0}{T_s(x) - T_m(x)} \tag{8}$$

where $T_s(x)$ and $T_m(x)$ are attributed to the tube wall temperature and fluid temperature, respectively. q^0 is known as the heat flux, and the convective heat transfer coefficient measured by employing and raising the temperature based on the flow rate adjustment to a stable state. The measured values were reported as average.

Results and discussion

Characterization of the nanoparticles

Figure 5 shows the FTIR spectra of the GO and NH_2-mGO. In the case of NH_2-mGO, the featured absorption band at 580 cm^{-1} should be attributed to the Fe–O bond vibration in the structure of the Fe_3O_4 located on the surface of the NH_2-mGO. Moreover, the absorption peak observed at 3433 cm^{-1} can be attributed to the O–H stretching, and 1625 cm^{-1} and 1200 cm^{-1} are attributed to the O–H bonding, and C–O stretching, respectively. The absorption peak observed around 2900 cm^{-1} is attributed to the C–H stretching in ethyl groups introduced on the graphene oxide surfaces. These observations confirmed the presence of magnetic and amino structures on the surface of the NH_2-mGO [51, 52].

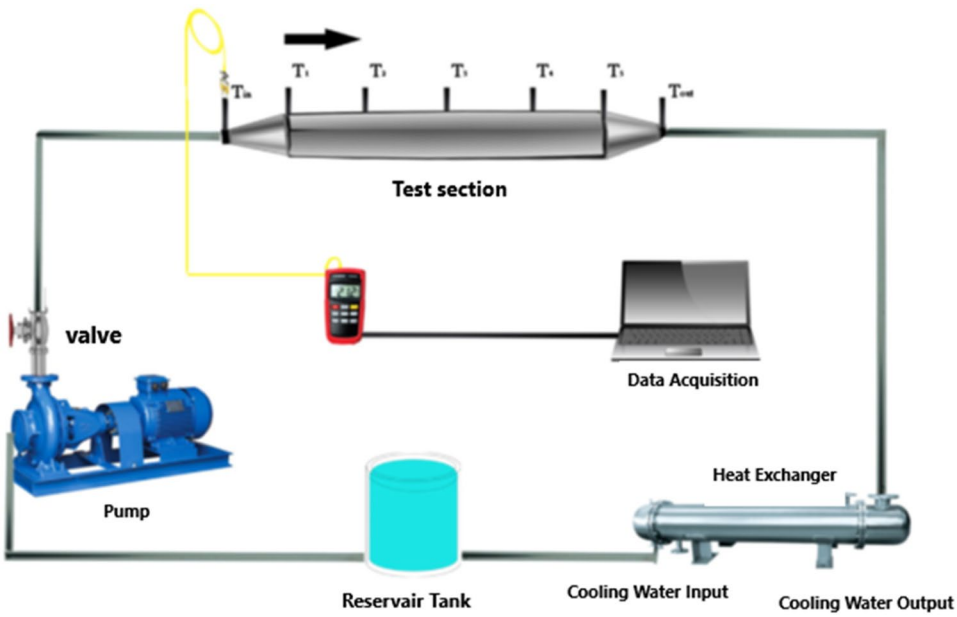

Fig. 4 Schematic design of the convective heat transfer

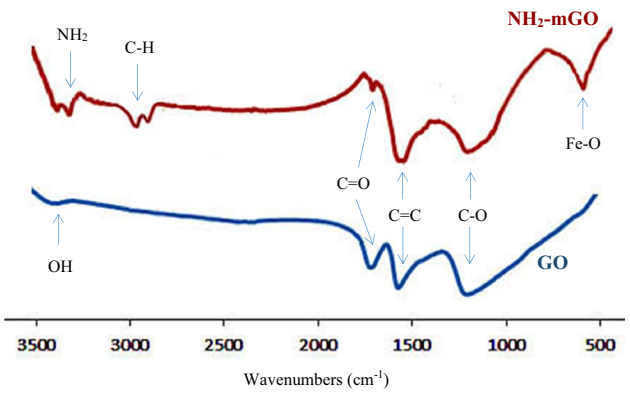

Fig. 5 FTIR spectrums of GO and NH2-mGO

The N_2 adsorption/desorption isotherms of GO and NH_2-mGO are presented in Fig. 6. The presence of mesopores confirmed in GO and NH_2-mGO structures. In the case of the NH_2-mGO, the mean pore diameter is 15.90 nm and the BET surface area decreased from 183.25 to 61.91 m^2/g because of the blocked pores after double modification of GO. The functionalization process blocked the pores available in the structure since amine groups and Fe_3O_4 nanoparticles are available in the pores. The BJH adsorption volume of the pores is determined as 0.2486 cm^3/g for NH_2-mGO [53].

The XRD patterns of the samples before and after double modification were studied. Figure 7 shows the XRD patterns of the GO and NH2-mGO. The peaks located at 2θ values of 18.2°, 30.3°, 35.1°, 43.2°, 57.3°, and 62.6° are related to the (1 1 1), (2 2 0), (3 1 1), (4 0 0), (4 2 2), (5 1 1) and (4 4 0) plans of Iron oxide, respectively. These results confirm the presence of Fe3O4 nanoparticles on the surface of the GO after the magnetization process. Moreover, the XRD pattern of the GO displays a peak located at $2\theta = 10.2°$, which is consistent with the other diffraction peaks observed for GO in different studies. After the magnetization process, the diffraction peak of the GO disappeared from the patterns of the NH2-mGO, confirming the transition of the GO into the graphene [54].

The SEM images of GO and NH_2-mGO are presented in Fig. 8. As shown, a more porous morphology is obtained for pristine GO before any modification. After modification with magnetic particles and amine groups, less porous morphology is obtained, and some of the pores were blocked because of the presence of Fe_3O_4 nanoparticles as well as amine groups. The lamellar structure was retained after double modification of the GO and Fe_3O_4 content available on the surface of the GO is confirmed, according to Fig. 8C and D [51].

Energy-dispersive X-ray spectroscopy (EDS) is used to study the structure of NH_2-mGO (Table 1). The presence of O, Fe, and N elements with weight percentages of 21.51, 9.43, and 5.61, indicates that graphene surfaces are well functionalized with ethylenediamine and magnetic Fe_3O_4 nanoparticles.

The TEM images of NH_2-mGO are presented in Fig. 9. As shown in Fig. 9A and B, NH_2-mGO particles are present in dimensions around 100 nm.

To study the stability of the nanofluids, a zeta potential analysis was employed. Zeta potential values more than ± 25 mV are desirable conditions to confirm the stability of nanostructures in the base fluid [28]. Figure 10 represents the measured zeta potential after 2 weeks of preparation of nanofluid. The zeta potential diagram revealed an average value of − 32.7 mV for the nanofluid containing NH_2-mGO as the nanoparticle added to the system. So, this potential

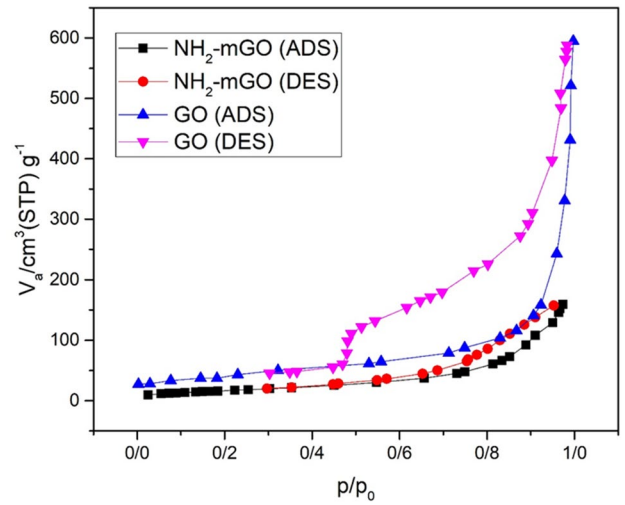

Fig. 6 BET adsorption/desorption of GO and NH2-mGO

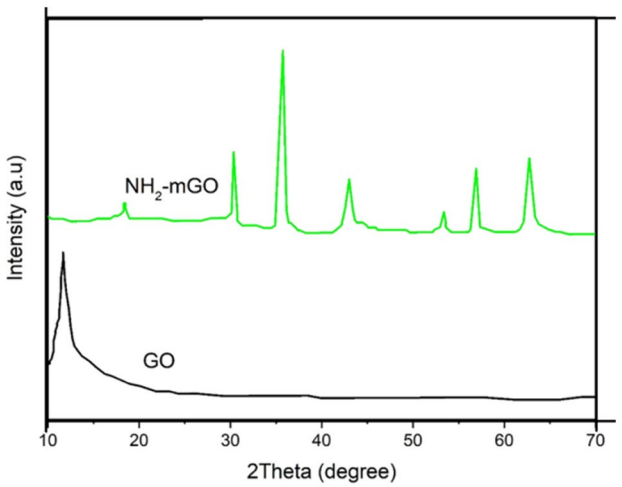

Fig. 7 XRD patterns of the GO and NH2-mGO (D)

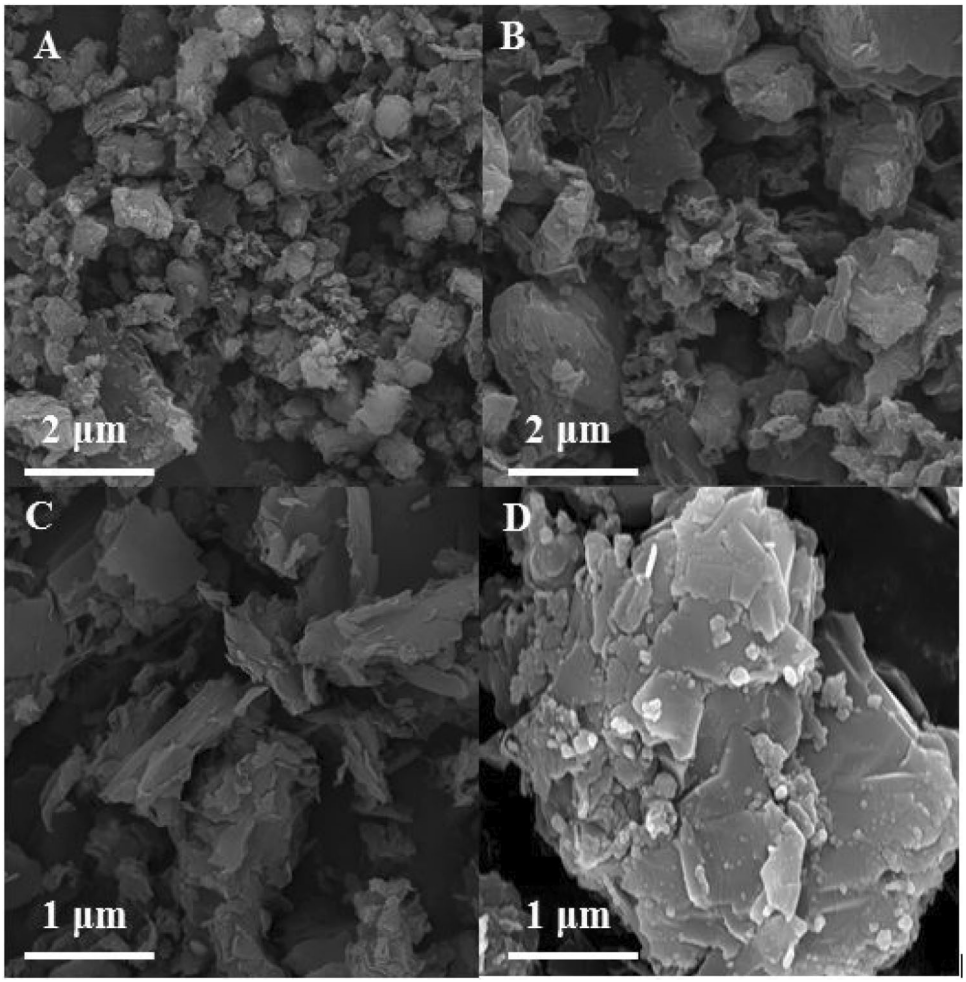

Fig. 8 SEM images of pristine GO (**A** and **B**) and NH2-mGO (**C** and **D**)

Table 1 Elements by weight percent using the EDS spectrum of GO and NH2-mGO

Element	GO		NH2-mGO	
	Weight%	Atomic%	Weight%	Atomic%
C K	85.18	87.73	63.45	67.70
O K	14.82	12.27	21.51	18.17
Fe K	–	–	9.43	8.82
N K	–	–	5.61	5.31
Totals	100.00	100.00	100.00	100.00

value confirmed the stability of NH_2-mGO nanoparticles in the base fluid to study the absorption experiments.

Figure 11 shows the results of XPS analysis. As shown, in the case GO, the two characteristic peaks at 284 and 529 eV correspond to C1s and O1s, respectively. The oxygen peak intensity is somewhat higher than the carbon peak intensity. The oxygen peak intensity is somewhat higher than the carbon peak intensity. Based on observations, the oxidation has been done successfully, and the presence of oxygen groups on the surface of graphene

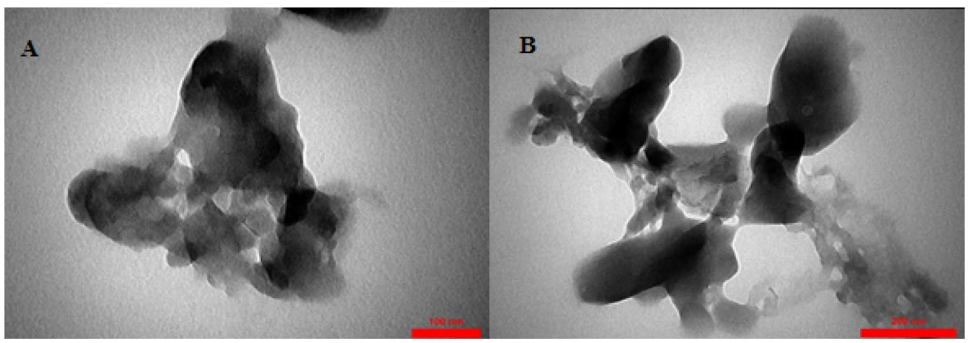

Fig. 9 TEM images of NH2-mGO

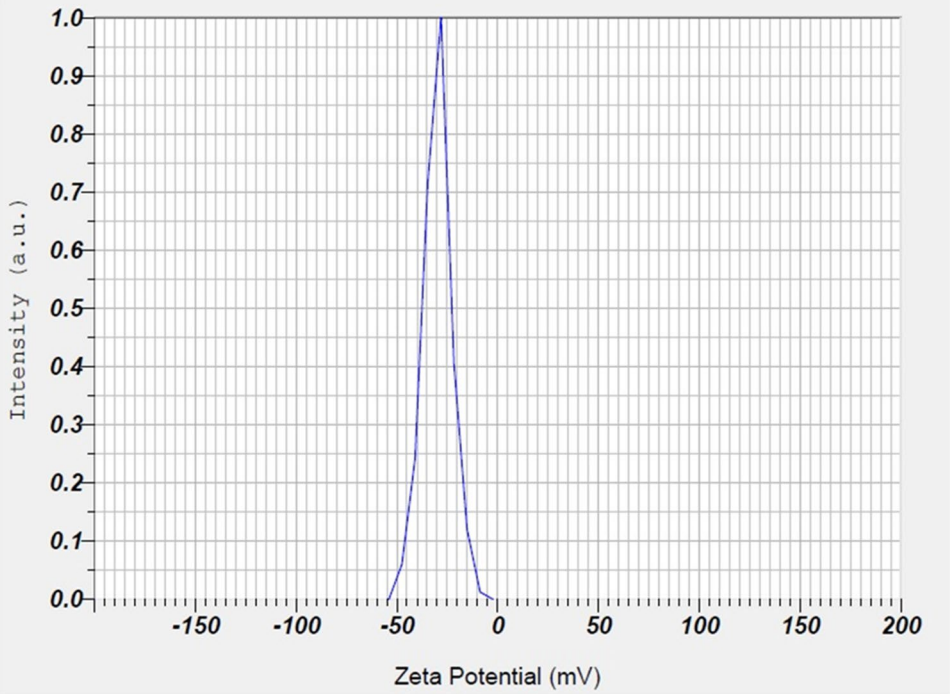

Fig. 10 Zeta potential diagram of the addition of 0.1 wt.% NH2-mGO to the 40 wt.% aqueous MDEA

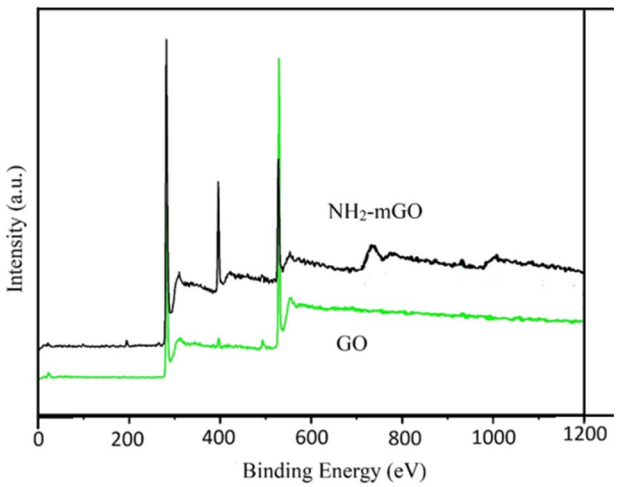

Fig. 11 XPS analysis of GO and NH2-mGO

oxide confirms these results. In the case of functionalized graphene oxide with iron oxide and amino groups, a new peak appears that is related to nitrogen (N1s). In this case, the intensity of the oxygen peak has decreased compared to graphene oxide, confirming the reaction of amine groups on the surface of graphene oxide and the lowering the intensity of oxygen groups. Another new peak observed at 720 EV is related to iron (2 p), which confirms the presence of magnetic nanoparticles in the structure of graphene oxide after chemical modification.

CO_2 absorption experiments

On our previous works to confirm the performance of our experimental setup, we compared the results obtained by our experimental system with the data reported by Shen et al. [55] and Mamun et al. [56]. The comparison confirmed the accuracy of the system [57].

We studied the absorption with the base fluid (40 wt.% aqueous MDEA solution), and nanofluids containing only graphene oxide at 303.15 K. Also, different dosages of the nanoparticles added to the base fluid were studied. The results are presented in Fig. 12.

As shown, for the nanofluid containing 0.1% and 0.2% of GO, the amount of carbon dioxide absorption increased by about 9.1% and 10.4%, respectively. The use of larger amounts of graphene oxide in the base fluid did not have a significant effect on carbon dioxide absorption, and we even saw a decrease in solubility in some cases. As shown, for all cases, the amount of carbon dioxide absorption increases significantly with the increase in the partial pressure of carbon dioxide. Based on these results, the optimum dosage of nanoparticles was determined as 0.1 wt.%. So, this optimum dosage was used for further absorption studies in this work.

The density of the as-prepared nanofluid was investigated by a Pycnometer at the different temperatures employed for CO_2 absorption experiments. 0.1 wt.% of the double modified GO added to 40 wt.% aqueous MDEA solution (as the base fluid) and density measurements were studied at 303.15, 313.15, 323.15 and 333.15 K. Table 2 shows the

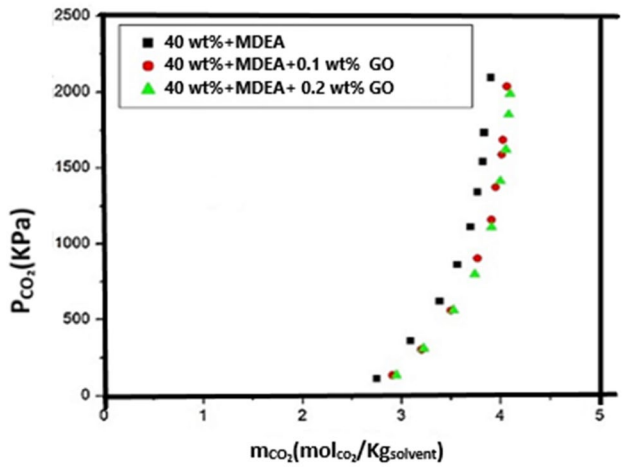

Fig. 12 CO2 absorption experiment for 40 wt.% MDEA solution and 40 wt.% MDEA solution containing 0.1 and 0.2% GO at 303.15 K

Table 2 The measured densities of nanofluid at desired temperatures (combined standard uncertainties Uc(ρ) = 0.00025 (g/cm3)

T (K)	ρ (40 wt.% MDEA + 0.1 wt.% NH2-mGO)
303.15	1.0394
313.15	1.0367
323.15	1.0321
333.15	1.0275

measured densities and confirm the reverse relationship between the density of the nanofluid and temperature.

In addition, CO_2 absorption was performed using 40 wt.% aqueous MDEA nanofluids containing zero and 0.1 wt.% NH_2-mGO nanoparticles. Figure 13 shows the results of the absorption experiments at different temperatures and pressures. As indicated, partial pressure has a positive effect on the CO_2 absorption capacity but, increasing the temperature resulted in a decrease in CO_2 absorption capacity. As shown, for nanofluid containing NH_2-mGO, the absorption capacity was enhanced up to 19% compared with 40 wt.% MDEA aqueous solution.

Mass diffusion (as a phenomenon) plays a critical role in nanofluids to enhance the mass transfer and gas absorption [45]. There are various studies performed on the mass transfer improvement in nanofluids due to the presence of the nanoparticles. The Brownian motion of the nanoparticles creates a velocity disturbance field in the base fluid resulting in mass diffusion enhancement. Another phenomenon regarding the nanofluid and mass transfer is considered as a grazing effect so that a thinner diffusion layer is created by the interaction of nanoparticles and gas–liquid interface. The gas–liquid interface is controlling the mass transfer between gas and liquid phases, and the diffusion rate should be dependent on the concentration gradient between the two sides of the gas film [58, 59]. Adsorption and desorption occurred on the surface of the nanoparticles are another reason to transport some amount of gas into the liquid bulk. Adsorption and desorption would occur in the diffusion layer and liquid bulk, respectively. So, a greater mass could be transferred resulted from an improvement in the mass transfer coefficient. CO_2 plays an anionic role in the presence of amine groups available on the surface of the nanoparticles. The interaction between the amine groups and CO_2 creates intermediates which are producing protonated groups and carbamate on the surface. So, CO_2 could be stabilized on the surface of the nanoparticles. The collision of the gas bubbles leads to small bubbles and increases surface area by cracked bubbles [60, 61]. This increased surface area results in increased absorption, as depicted in Fig. 14.

Table 3 compares the results obtained on this research with the similar works. As shown, for all cases, (different nanoparticles added to the different fluids) there is significant enhancement in the CO_2 absorption. The enhancement observed in this work is comparable with the other works presented on the table, however, the easy regeneration of the nanoparticles and reuse of the solution is the advantage of our work [21, 62–67].

CO_2 absorption performance of recycled NH_2-mGO through five cycles

When CO_2 absorption experiments competed, the NH_2-mGO recovered by a magnet and recycled nanoparticles were then degassed at 150 °C under vacuum overnight. The obtained nanoparticles were added to the base fluid, and experiments performed at 303.15 K through multiple cycles. As shown in Fig. 15, NH_2-mGO has the ability to effectively recover and retain its active sites on the surface throughout the repeated cycles and thermal treatment.

Thermal conductivity measurements

Thermal conductivity of the nanofluid and base fluid were measured at various temperatures ranged from 298 to 328 K. A thermostat bath was used to study the effect of the temperature on the effective thermal conductivity at desired temperatures employed for absorption experiments. As shown in Fig. 16, the addition of nanoparticles led to an increase in effective thermal conductivity (K_{eff}) compared to the based fluid and increasing the temperature increased the thermal conductivity because of the presence of nanoparticles.

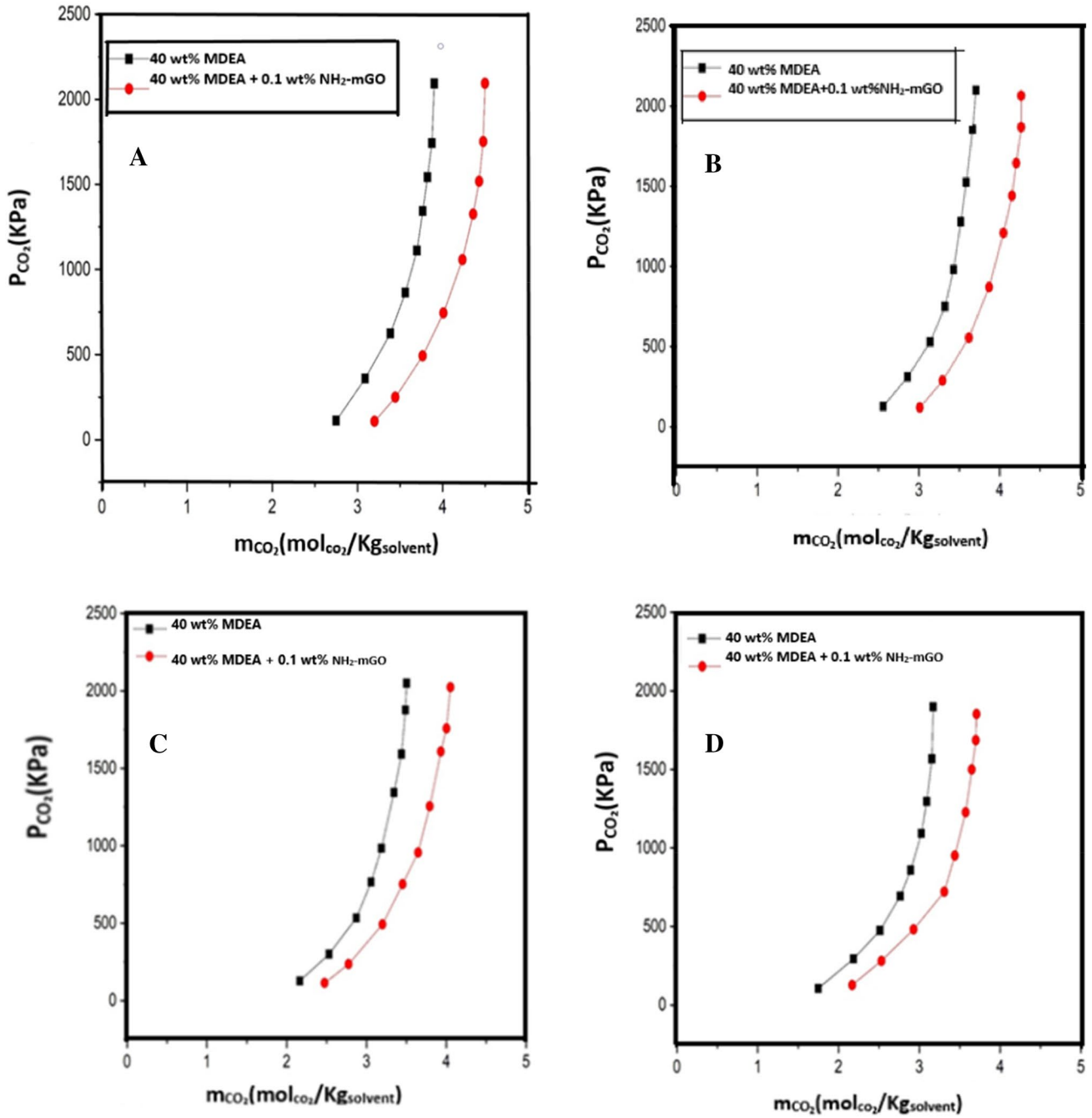

Fig. 13 CO2 absorption experiment for 40 wt.% MDEA solution and 40 wt.% MDEA solution containing 0.1 wt.% NH2-mGO at different temperatures A(303.15), B(313.15),C(323.15), D (333.15)

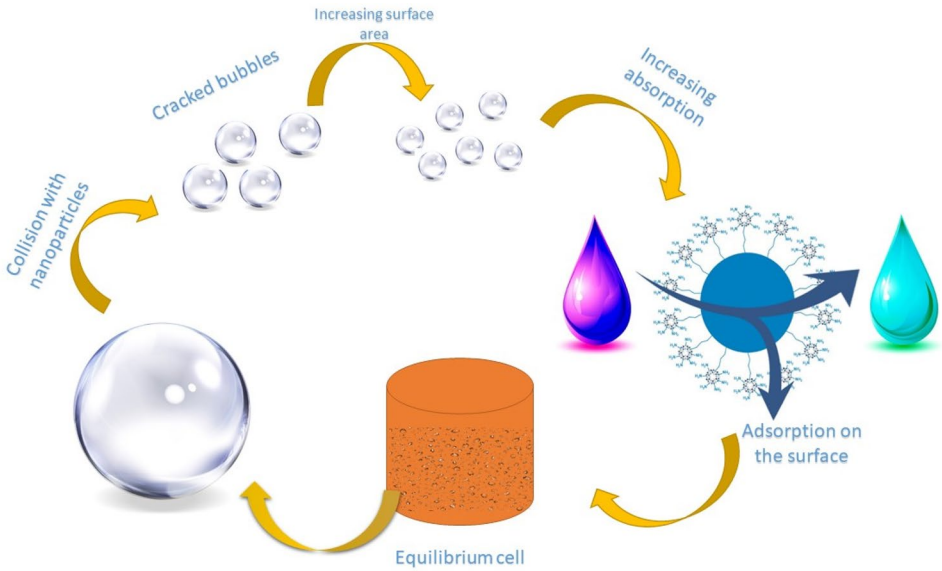

Fig. 14 Collision of the gas bubbles with nanoparticle and cracked bubbles

Table 3 Comparing the results with the similar works

Nano particles	%wt	Base fluid	CO2 absorption	Ref.
This work	0.1%	MDEA	19%	
TiO2	0.8%	MDEA	11.52%	[62]
NH2-rGO	0.1%	MDEA	16.2%	[21]
Al2O3	0.01%	NaCl-H2O	12.5%	[63]
Silica(SiO2)	0.021%	Piperazne/K2O3	12%	[64]
Al2O3	0.05%	Methanol	4.9%	[65]
SiO2	0.05%	Methanol	9.7%	[65]
CNT	0.02%	Pure water	34%	[66]
Fe3O4	0.02%	Pure water	24%	[66]
Al2O3	0.1%	Pure water	18%	[66]
SiO2	0.1%	Pure water	21%	[66]
CNT	0.02%	MDEA	23%	[66]

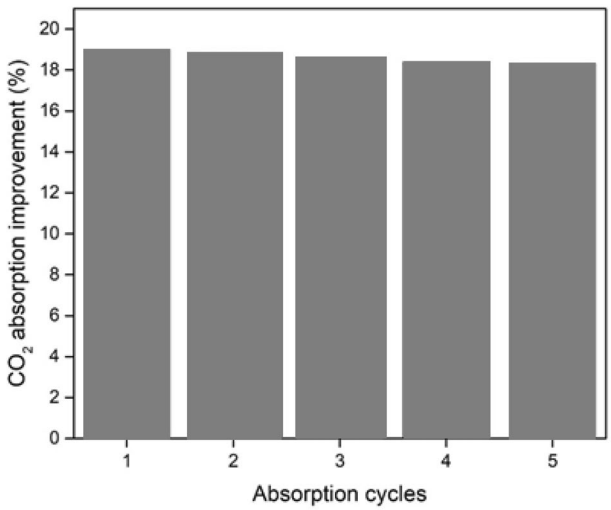

Fig. 15 CO2 absorption cycles at 303.15 K for the addition of 0.1 wt.% NH2-mGO into 40 wt.% MDEA after recycling by a magnet

Heat transfer is known as one of the key factors in industrial sections as well as the gas sweetening processed [50]. Improving the heat transfer in the gas sweetening processes could efficiently affect the cost and energy consumption. For this purpose, convective heat transfer was investigated in the NH_2-mGO nanofluid by changing the Reynolds number. Figure 17 shows the measured convective heat transfer coefficient. As shown, the convective heat transfer coefficient was improved up to 10–20% after the addition of nanoparticles. Increasing the Reynolds number has a positive effect on the measured convective heat transfer values. So, nanoparticles effectively enhanced the heat transfer properties of the fluids.

Conclusions

Amino functionalized magnetic graphene oxide was synthesized and added to the 40 wt.% aqueous MDEA to enhance CO_2 absorption capacity, thermal conductivity, and convective heat transfer. CO_2 absorption experiments showed a 19% enhancement compared with the base fluid. The spent nanostructure was recovered by a magnet through five cycles, and CO_2 absorption results revealed an acceptable performance associated with NH_2-mGO after five cycles. The presence of the nanostructure in the base fluid leads to 17% increase in thermal conductivity compared to the base fluid. Convective heat transfer results at different Reynolds numbers confirmed

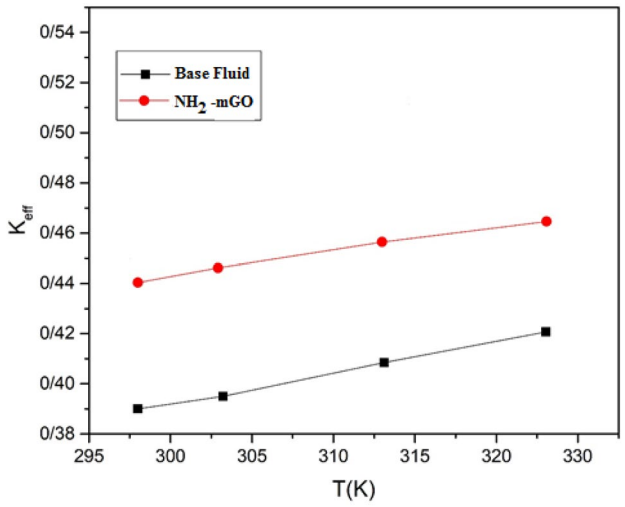

Fig. 16 Effective thermal conductivity of nanofluid and base fluid at various temperatures

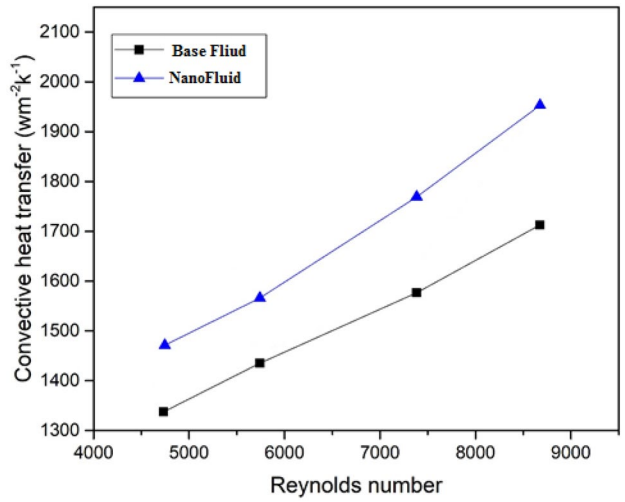

Fig. 17 Measured convective heat transfer coefficient for the base fluid and NH2-mGO nanofluid

an average enhancement (by 15%) in the heat transfer coefficient. NH_2-mGO could be used as a low-cost, green, and regenerable additive in amine-based solutions to enhance the gas absorption capacity as well as heat and mass transfer properties.

References

1. M. Arshadi, H. Taghvaei, M.K. Abdolmaleki, M. Lee, H. Eskandarloo, A. Abbaspourrad, Carbon dioxide absorption in water/nano fl uid by a symmetric amine-based nanodendritic adsorbent. Appl. Energy. **242**, 1562–1572 (2019). https://doi.org/10.1016/j.apenergy.2019.03.105
2. T. Wang, J. Liu, H. Huang, M. Fang, Z. Luo, Preparation and kinetics of a heterogeneous sorbent for CO2 capture from the atmosphere. Chem. Eng. J. (2016). https://doi.org/10.1016/j.cej.2015.09.009
3. F.D. Meylan, V. Moreau, S. Erkman, CO2 utilization in the perspective of industrial ecology, an overview. J. Util. (2015). https://doi.org/10.1016/j.jcou.2015.05.003
4. R.M. Cuéllar-Franca, A. Azapagic, Carbon capture, storage and utilisation technologies: a critical analysis and comparison of their life cycle environmental impacts. J. CO2 Util. **9**, 82–102 (2015). https://doi.org/10.1016/j.jcou.2014.12.001
5. T.M. McDonald, J.A. Mason, X. Kong, E.D. Bloch, D. Gygi, A. Dani, V. Crocellà, F. Giordanino, S.O. Odoh, W.S. Drisdell, B. Vlaisavljevich, A.L. Dzubak, R. Poloni, S.K. Schnell, N. Planas, K. Lee, T. Pascal, L.F. Wan, D. Prendergast, J.B. Neaton, B. Smit, J.B. Kortright, L. Gagliardi, S. Bordiga, J.A. Reimer, J.R. Long, Cooperative insertion of CO2 in diamine-appended metal-organic frameworks. Nature (2015). https://doi.org/10.1038/nature14327
6. T. Best, K.N. Finney, D.B. Ingham, M. Pourkashanian, CO2-enhanced and humidified operation of a micro-gas turbine for carbon capture. J. Clean. Prod. **176**, 370–381 (2018). https://doi.org/10.1016/j.jclepro.2017.12.062
7. S. Singto, T. Supap, R. Idem, P. Tontiwachwuthikul, S. Tantayanon, M.J. Al-Marri, A. Benamor, Synthesis of new amines for enhanced carbon dioxide (CO2) capture performance: the effect of chemical structure on equilibrium solubility, cyclic capacity, kinetics of absorption and regeneration, and heats of absorption and regeneration. Sep. Purif. Technol. **167**, 97–107 (2016). https://doi.org/10.1016/j.seppur.2016.05.002
8. C. Goel, H. Bhunia, P.K. Bajpai, Novel nitrogen enriched porous carbon adsorbents for CO2 capture: breakthrough adsorption study. J. Environ. Chem. Eng. **4**, 346–356 (2016). https://doi.org/10.1016/j.jece.2015.11.017
9. M.A. Sakwa-Novak, C.J. Yoo, S. Tan, F. Rashidi, C.W. Jones, Poly(ethylenimine)-functionalized monolithic alumina honeycomb adsorbents for CO2 capture from air. Chemsuschem (2016). https://doi.org/10.1002/cssc.201600404
10. A.D. Boyd, J.D. Hmielowski, P. David, Public perceptions of carbon capture and storage in Canada: results of a national survey. Int. J. Greenh. Gas Control. **67**, 1–9 (2017). https://doi.org/10.1016/j.ijggc.2017.10.010
11. M. Rezakazemi, M. Sadrzadeh, T. Matsuura, Thermally stable polymers for advanced high-performance gas separation membranes. Prog. Energy Combust. Sci. **66**, 1–41 (2018). https://doi.org/10.1016/j.pecs.2017.11.002
12. S.K. Dash, S.S. Bandyopadhyay, Studies on the effect of addition of piperazine and sulfolane into aqueous solution of N-methyldiethanolamine for CO2 capture and VLE modelling using eNRTL equation. Int. J. Greenh. Gas Control. **44**, 227–237 (2016). https://doi.org/10.1016/j.ijggc.2015.11.007
13. Y. Shen, H. Wang, J. Liu, Y. Zhang, Enhanced performance of a novel polyvinyl amine/chitosan/graphene oxide mixed matrix membrane for CO<inf>2</inf> capture. ACS Sustain. Chem. Eng. (2015). https://doi.org/10.1021/acssuschemeng.5b00409
14. E.A. Feijani, H. Mahdavi, A. Tavasoli, Poly(vinylidene fluoride) based mixed matrix membranes comprising metal organic frameworks for gas separation applications. Chem. Eng. Res. Des. **96**, 87–102 (2015). https://doi.org/10.1016/j.cherd.2015.02.009
15. A.-H. Lu, G.-P. Hao, X.-Q. Zhang, *Porous materials for carbon dioxide capture* (Springer, Berlin, 2014). https://doi.org/10.1007/978-3-642-54646-4
16. C.F. Martín, M.B. Sweatman, S. Brandani, X. Fan, Wet impregnation of a commercial low cost silica using DETA for a fast

post-combustion CO2 capture process. Appl. Energy. **183**, 1705–1721 (2016). https://doi.org/10.1016/j.apenergy.2016.09.081
17. K.S.N. Kamarudin, N. Zaini, N.E.A. Khairuddin, CO2removal using amine-functionalized kenaf in pressure swing adsorption system. J. Environ. Chem. Eng. **6**, 549–559 (2018). https://doi.org/10.1016/j.jece.2017.12.040
18. M.H. Ghasemi, V. Irani, A. Tavasoli, Amino functionalized ZIF-90@GO/MDEA nanofluid: As a new class of multi-hybrid systems to enhance the performance of amine solutions in CO2 absorption. J. Nat. Gas Sci. Eng. **74**, 103110 (2020). https://doi.org/10.1016/j.jngse.2019.103110
19. A. Maleki, V. Irani, A. Tavasoli, H2S solubility enhancement using ethylene diamine functionalized carbon nanotubes and the aqueous solution of N-methyldiethanolamine. J. Nat. Gas Sci. Eng. **71**, 103004 (2019). https://doi.org/10.1016/j.jngse.2019.103004
20. V. Irani, A. Maleki, A. Tavasoli, CO2 absorption enhancement in graphene-oxide/MDEA nanofluid. J. Environ. Chem. Eng. **7**, 102782 (2019). https://doi.org/10.1016/j.jece.2018.11.027
21. V. Irani, A. Tavasoli, M. Vahidi, Preparation of amine functionalized reduced graphene oxide/methyl diethanolamine nanofluid and its application for improving the CO2 and H2S absorption. J. Colloid Interface Sci. (n.d.). (2018). https://doi.org/10.1016/j.jcis.2018.05.018
22. R. Aghehrochaboki, Y. Aghdoud Chaboki, S.A. Maleknia, V. Irani, Polyethyleneimine functionalized graphene oxide/methyldiethanolamine nanofluid: Preparation, characterization, and investigation of CO2 absorption. J. Environ. Chem. Eng. **7**, 103285 (2019). https://doi.org/10.1016/j.jece.2019.103285
23. V. Irani, A. Tavasoli, A. Maleki, M. Vahidi, Polyethyleneimine-functionalized HKUST-1/MDEA nanofluid to enhance the absorption of CO2in gas sweetening process. Int. J. Hydrogen Energy. **43**, 5610–5619 (2018). https://doi.org/10.1016/j.ijhydene.2018.01.120
24. J. Pokhrel, N. Bhoria, S. Anastasiou, T. Tsou, Microporous and Mesoporous Materials CO2 adsorption behavior of amine-functionalized ZIF-8, graphene oxide and ZIF-8/graphene oxide composites under dry and wet conditions. Microporous Mesoporous Mater. **267**, 53–67 (2018). https://doi.org/10.1016/j.micromeso.2018.03.012
25. N.A. Rashidi, S. Yusup, An overview of activated carbons utilization for the post-combustion carbon dioxide capture. J CO2 Util. **13**, 1–16 (2016). https://doi.org/10.1016/j.jcou.2015.11.002
26. B. Ghalei, K. Sakurai, Y. Kinoshita, K. Wakimoto, A.P. Isfahani, Q. Song, K. Doitomi, S. Furukawa, H. Hirao, H. Kusuda, S. Kitagawa, E. Sivaniah, Enhanced selectivity in mixed matrix membranes for CO2capture through efficient dispersion of amine-functionalized MOF nanoparticles. Nat. Energy (2017). https://doi.org/10.1038/nenergy.2017.86
27. B. Szczęśniak, J. Choma, M. Jaroniec, Gas adsorption properties of graphene-based materials. Adv. Colloid Interface Sci. **243**, 46–59 (2017). https://doi.org/10.1016/j.cis.2017.03.007
28. M. Vahidi, A. Tavasoli, A.M. Rashidi, Preparation of amine functionalized UiO-66, mixing with aqueous N-Methyldiethanolamine and application on CO2 solubility. J. Nat. Gas Sci. Eng. **28**, 651–659 (2016). https://doi.org/10.1016/j.jngse.2015.11.050
29. A. Maleki, V. Irani, A. Tavasoli, M. Vahidi, Enhancement of CO2solubility in a mixture of 40 wt% aqueous N-Methyldiethanolamine solution and diethylenetriamine functionalized graphene oxide. J. Nat. Gas Sci. Eng. **55**, 219–234 (2018). https://doi.org/10.1016/j.jngse.2018.04.032
30. R. Saidur, K.Y. Leong, H.A. Mohammad, A review on applications and challenges of nanofluids. Renew. Sustain. Energy Rev. **15**, 1646–1668 (2011). https://doi.org/10.1016/j.rser.2010.11.035
31. A. Arshad, M. Jabbal, Y. Yan, D. Reay, A review on graphene based nanofluids : preparation, characterization and applications particle size synthesis method preparation method distilled water liquid paraffin. J. Mol. Liq. **279**, 444–484 (2019). https://doi.org/10.1016/j.molliq.2019.01.153
32. M. Irani, M.M. Ghafurian, M.M. Khorasani, R. Mehrkhah, O. Mahian, A comparative study of the effect of phase change material (paraffin wax) on volumetric and surface direct solar steam generation. Engineers. **128**, 253–260 (2021). https://doi.org/10.1016/j.jtice.2021.07.046
33. K. Goharshadi, S.A. Sajjadi, E.K. Goharshadi, R. Mehrkhah, A review on applications and challenges of nanofluids. Mater. Res. Bull. **15**, 1646–1668 (2011). https://doi.org/10.1016/j.materresbull.2022.111916
34. R. Mehrkhah, M.M. Ghafurian, H. Niazmand, E.K. Goharshadi, O. Mahian, The use of nanofluids in solar desalination of saline water resources as antibacterial agents, in *Advances in nanofluid heat transfer*. ed. by H.M. Ali (Elsevier, New York, 2022), pp.265–301. https://doi.org/10.1016/B978-0-323-88656-7.00009
35. M.K. Nazarabad, H.A. Toupkanloo, Functionalization of beet waste by cross-linking to attach amine groups for efficient sorption of reactive black 5 anionic dye. J. Iran. Chem. Soc. **19**, 1525–2537 (2022). https://doi.org/10.1007/s13738-021-02398-3
36. E.K. Goharshadi, H.A. Toupkanloo, M. Karimi, Electrical conductivity of water-based palladium nanofluids. Microfluid. Nanofluid. **18**, 667–672 (2015). https://doi.org/10.1007/s10404-014-1465-0
37. M. Nabipour, P. Keshavarz, S. Raeissi, Experimental investigation on CO2 absorption in sulfinol-M based Fe3O4 and MWCNT nanofluids. Int. J. Refrig. **73**, 1–10 (2017). https://doi.org/10.1016/j.ijrefrig.2016.09.010
38. H. Mohammaddoost, A. Azari, M. Ansarpour, S. Osfouri, Experimental investigation of CO2removal from N2by metal oxide nanofluids in a hollow fiber membrane contactor. Int. J. Greenh. Gas Control. **69**, 60–71 (2018). https://doi.org/10.1016/j.ijggc.2017.12.012
39. S.S. Ashrafmansouri, M. Nasr Esfahany, Mass transfer in nanofluids: A review. Int. J. Therm. Sci. **82**, 84–90 (2014). https://doi.org/10.1016/j.ijthermalsci.2014.03.017
40. S. Nallusamy, Characterization of Al2O3/water nanofluid through shell and tube heat exchangers over parallel and counter flow. J. Nano Res. **45**, 155–163 (2017). https://doi.org/10.4028/www.scientific.net/JNanoR.45.155
41. S. Nallusamy, Thermal conductivity analysis and characterization of copper oxide nanofluids through different techniques. J. Nano Res. **40**, 102–112 (2015). https://doi.org/10.4028/www.scientific.net/JNanoR.40.105
42. X. Cai, M. Lin, S. Tan, W. Mai, Y. Zhang, Z. Liang, Z. Lin, X. Zhang, The use of polyethyleneimine-modified reduced graphene oxide as a substrate for silver nanoparticles to produce a material with lower cytotoxicity and long-term antibacterial activity. Carbon **50**, 3407–3415 (2012). https://doi.org/10.1016/j.carbon.2012.02.002
43. L. Chen, D. Zhao, S. Chen, X. Wang, C. Chen, One-step fabrication of amino functionalized magnetic graphene oxide composite for uranium(VI) removal. J. Colloid Interface Sci. **472**, 99–107 (2016). https://doi.org/10.1016/j.jcis.2016.03.044
44. A. Maleki, U. Hamesadeghi, H. Daraei, B. Hayati, F. Najafi, G. McKay, R. Rezaee, Amine functionalized multi-walled carbon nanotubes: single and binary systems for high capacity dye removal. Chem. Eng. J. (2016). https://doi.org/10.1016/j.cej.2016.10.058
45. C. Pang, J.W. Lee, Y.T. Kang, Review on combined heat and mass transfer characteristics in nanofluids. Int. J. Therm. Sci. **87**, 49–67 (2015). https://doi.org/10.1016/j.ijthermalsci.2014.07.017
46. M.H. Jenab, M.A. Abdi, S.H. Najibi, M. Vahidi, N.S. Matin, N. Iranian, O. Company, Solubility of carbon dioxide in aqueous

mixtures of N-methyldiethanolamine+ piperazine+ sulfolane. J. Chem. Eng. Data **50**, 583–586 (2005). https://doi.org/10.1021/je049666p
47. M.K. Park, O.C. Sandall, Solubility of carbon dioxide and nitrous oxide in 50 mass % methyldiethanolamine. J. Chem. Eng. Data. **46**, 166–168 (2001). https://doi.org/10.1021/je000190t
48. G. Xu, C. Zhang, S. Qin, Y. Wang, Kinetics study on absorption of carbon dioxide into solutions of activated methyldiethanolamine. Ind. Eng. Chem. Res. **31**, 921–927 (1992). https://doi.org/10.1021/ie00003a038
49. M. Vahidi, A. Rashidi, A. Tavasoli, S. Kiani, Remarkable enhancement of convective heat transfer with different nanoparticles in N-methyldiethanolamine solution in gas sweetening process. Int. Commun. Heat Mass Transf. **76**, 1–5 (2016). https://doi.org/10.1016/j.icheatmasstransfer.2016.05.016
50. M. Vahidi, A. Rashidi, A. Tavasoli, S. Kiani, Remarkable enhancement of convective heat transfer with different nanoparticles in N -methyldiethanolamine solution in gas sweetening process ☆. Int. Commun. Heat Mass Transf. **76**, 1–5 (2016). https://doi.org/10.1016/j.icheatmasstransfer.2016.05.016
51. L. Cui, Y. Wang, L. Gao, L. Hu, L. Yan, Q. Wei, B. Du, EDTA functionalized magnetic graphene oxide for removal of Pb (II), Hg (II) and Cu (II) in water treatment : adsorption mechanism and separation property. Chem. Eng. J. **281**, 1–10 (2015). https://doi.org/10.1016/j.cej.2015.06.043
52. F. Reguyal, A.K. Sarmah, Adsorption of sulfamethoxazole by magnetic biochar: Effects of pH, ionic strength, natural organic matter and 17α-ethinylestradiol. Sci. Total Environ. **628–629**, 722–730 (2018). https://doi.org/10.1016/j.scitotenv.2018.01.323
53. M. Dastkhoon, M. Ghaedi, A. Asfaram, R. Jannesar, F. Sadeghfar, Magnetic based nanocomposite sorbent combination with ultrasound assisted for solid-phase microextraction of Azure II in water samples prior to its determination spectrophotometric. J. Colloid Interface Sci. **513**, 240–250 (2018). https://doi.org/10.1016/j.jcis.2017.11.031
54. X. Guo, B. Du, Q. Wei, J. Yang, L. Hu, L. Yan, W. Xu, Synthesis of amino functionalized magnetic graphenes composite material and its application to remove Cr(VI), Pb(II), Hg(II), Cd(II) and Ni(II) from contaminated water. J. Hazard. Mater. **278**, 211–220 (2014). https://doi.org/10.1016/j.jhazmat.2014.05.075
55. K.-P. Shen, M.-H. Li, Solubility of carbon dioxide in aqueous mixtures of monoethanolamine with methyldiethanolamine. J. Chem. Eng. Data. **37**, 96–100 (1992). https://doi.org/10.1021/je00005a025
56. S. Ma'mun, R. Nilsen, H.F. Svendsen, O. Juliussen, Solubility of carbon dioxide in 30 mass % monoethanolamine and 50 mass % methyldiethanolamine solutions. J. Chem. Eng. Data. **50**, 630–634 (2005). https://doi.org/10.1021/je0496490
57. V. Irani, A. Maleki, A. Tavasoli, CO2 absorption enhancement in graphene-oxide/MDEA nanofluid. J. Environ. Chem. Eng. (2018). https://doi.org/10.1016/j.jece.2018.11.027
58. X. Ma, F. Su, J. Chen, T. Bai, Z. Han, Enhancement of bubble absorption process using a CNTs-ammonia binary nanofluid. Int. Commun. Heat Mass Transf. **36**, 657–660 (2009). https://doi.org/10.1016/j.icheatmasstransfer.2009.02.016
59. M. Darabi, M. Rahimi, A. Molaei Dehkordi, Gas absorption enhancement in hollow fiber membrane contactors using nanofluids: modeling and simulation. Chem. Eng. Process. Process Intensif. **119**, 7–15 (2017). https://doi.org/10.1016/j.cep.2017.05.007
60. J.W. Lee, I.T. Pineda, J.H. Lee, Y.T. Kang, Combined CO2absorption/regeneration performance enhancement by using nanoabsorbents. Appl. Energy. **178**, 164–176 (2016). https://doi.org/10.1016/j.apenergy.2016.06.048
61. M. Bahiraei, S. Heshmatian, Graphene family nano fl uids : a critical review and future research directions. Energy Convers. Manag. **196**, 1222–1256 (2019). https://doi.org/10.1016/j.enconman.2019.06.076
62. Sh. Li, Y. Ding, X. Zhang, Enhancement on CO_2 bubble absorption in MDEA solution by TiO_2 nanoparticles. Adv Mater Res **631–631**, 127–134 (2013). https://doi.org/10.4028/www.scientific.net/AMR.631-632.127
63. J.W. Lee, Y.T. Kang, CO_2 absorption enhancement by Al_2O_3 nanoparticles in NaCl aqueous solution. Energy **53**, 206–211 (2013). https://doi.org/10.1016/j.energy.2013.02.047
64. W.-G. Kim, H.U. Kang, K.-M. Jung, S.H. Kim, Synthesis of silica nanofluid and application to CO_2 absorption. Sep. Sci. Technol. **43**, 3036–3035 (2008). https://doi.org/10.1080/01496390802063804
65. I.T. Pineda, J.W. Lee, I. Jung, Y.T. Kang, CO_2 absorption enhancement by methanol-based Al_2O_3 and SiO_2 nanofluids in a tray column absorber. Int. J. Refrig **35**, 1402–1409 (2012). https://doi.org/10.1016/j.ijrefrig.2012.03.017
66. B. Rahmatman, P. Keshavarz, Sh. Ayatollahi, Study of absorption enhancement of CO2 by SiO2, Al2O3, CNT, and Fe3O4 nanoparticles in water and amine solutions. J. Chem. Eng **61**, 1378–1387 (2016). https://doi.org/10.1021/acs.jced.5b00442
67. N. Mehmandost, N. Goudarzi, M.A. Chamjangali, G. Bagherian, Removal of methylene blue and crystal violet in binary aqueous solution by magnetic Terminalia catappa kernel shell biosorbent using Box-Behnken design. J. Iran. Chem. Soc. **19**, 3769–3781 (2022). https://doi.org/10.1007/s13738-022-02552-5